Advanced Review

Nanoimaging for protein misfolding diseases

Yuri L. Lyubchenko,* Bo-Hyun Kim, Alexey V. Krasnoslobodtsev and Junping Yu

Misfolding and aggregation of proteins are widespread phenomena leading to the development of numerous neurodegenerative disorders such as Parkinson's, Alzheimer's, and Huntington's diseases. Each of these diseases is linked to structural misfolding and aggregation of a particular protein. The aggregated forms of the protein induce the development of a particular disease at all levels, leading to neuronal dysfunction and loss. Because protein refolding is frequently accompanied by transient association of partially folded intermediates, the propensity to aggregate is considered a general characteristic of the majority of proteins. X-ray crystallography, nuclear magnetic resonance, electron microscopy, and atomic force microscopy have provided important information on the structure of aggregates. However, fundamental questions, such as why the misfolded conformation of the protein is formed, and why this state is important for self-assembly, remain unanswered. Although it is well known that the same protein under pathological conditions can lead to the formation of aggregates with diverse biological consequences, the conditions leading to misfolding and the formation of the disease prone complexes are unclear, complicating any development of efficient prevention of the diseases. Misfolded states exist transiently, so answering these questions requires the use of novel approaches and methods. Progress has been made during the past few years, when recently developed ensemble methods and single-molecule biophysics techniques were applied to the problem of the protein misfolding. In this review, the impacts of these studies on the understanding of the mechanisms of the protein self-assembly into aggregates and on the development of treatments of the diseases are discussed. *WIREs Nanomed Nanobiotechnol* 2010 2 526–543

PROTEIN AGGREGATES AND DISEASES

Misfolding and aggregation of proteins are fundamental phenomena of protein biophysics leading to the development of a number of devastating neurodegenerative diseases, including Alzheimer's (AD), Parkinson's, and Huntington's diseases, amyotrophic lateral sclerosis, frontal temporal dementia, and the human prion diseases.[1] The accumulation of abnormal protein aggregates detected as extracellular or intracellular deposits represents a common pathological signature for these diverse neurodegenerative disorders. Proteins from such deposits can spontaneously assemble into aggregates in test tubes, and this finding dramatically facilitated physical, chemical, and structural analysis of protein aggregates. Studies during past decade, with the use of such techniques as X-ray fibril diffraction,[2] electron microscopy (EM),[3] and atomic force microscopy (AFM),[4–6] as well as spectroscopic methods,[7,8] showed that misfolded proteins are assembled into fibrils with a periodic structure, stabilized by β-sheet structural motifs. An early model proposed by M.F. Perutz et al.[9] was based on X-ray diffraction studies that explained the organization of poly-glutamine peptides constituting the core of huntingtin, the aggregation of which is responsible for the development of Huntington's disease. In this water-filled nanotube model, the polypeptide chains fold to β-strands that form a cylindrical sheet of 3 nm diameter, forming a hollow cylinder filled with water. Proposed first for the fibrils formed by poly Gln polymer (a model system for Huntington's

*Correspondence to: ylyubchenko@unmc.edu

Department of Pharmaceutical Sciences, University of Nebraska Medical Center, Omaha, NE 68198-6025, USA

DOI: 10.1002/wnan.102

protein),[10] the model was also used to explain the peculiarities of the fibril structure of amyloid β (Aβ) peptide, α-synuclein, and prion proteins. At the same time, assembly of proteins into fibrillar aggregates prevented the use of such high-resolution structural method as X-ray crystallography, and this fact dramatically impeded high-resolution structural analysis of protein nanofibrils with atomic resolution. The breakthrough was made in the laboratory of D. Eisenberg, in which the crystallographic structure of short peptide (GNNQQNY peptide) from the yeast prion protein Sup35 was obtained.[11] These studies have identified several (eight) classes of so-called steric zippers. Despite the fundamental similarities in the structure with extended protein strands that are perpendicular to the axis of β-sheets, these classes vary in the basic steric zipper structure. Such variation mainly involves the orientation of peptides and β-sheets with respect to each other. It was found that some peptides were capable of forming different polymorphs with regard to their basic steric zipper structure, offering a possible explanation for amyloid polymorphism and prion strains.[11]

Note a fundamental contribution to the structural analysis of amyloid fibrils made by the use of solid-state NMR (SS-NMR) (reviewed in Ref 12). A structural model for amyloid fibrils formed by the 40-residue Aβ peptide was proposed based on the results of the SS-NMR spectroscopy.[13–15] These studies showed that the first 10 residues of Aβ (1–40) within the fibril are not structured; however, the rest of the protein, except for the 25–29 region, adopts an antiparallel β-sheet conformation. Residues 25–29 contain a bend of the peptide backbone that brings the two β-strands in contact, forming β-sheet (hairpin structure) through side chain–side chain interactions.

Based on SS-NMR and X-ray crystallography, the underlying structure of prion amyloids was found to share common structural features. They contain similarly arranged parallel β-sheets that are packed in-register for a variety of different prion proteins, such as Ure2p1-89 (the basis of the [URE3] prion),[16] Ure2p10-39,[17] Sup35p ([PSI+] prion),[18] and Rnq1p ([PIN+] prion).[19] Generally, β-strands of a protein molecule run perpendicular to the axis of the fibril, and hydrogen bonding in such structures occurs along the length of the fibril.

The studies performed with other proteins lead to a general picture, where individual polypeptide chains are stacked in-register, forming parallel β-sheets oriented perpendicular to the major axis of the fibril. However, recent studies showed that this picture, especially when it applies to proteins such as α-synuclein and yeast prions HET-s and Ure2p, should be replaced with a more complex one, in which a part of the polypeptide chain in amyloid fibrils remains intrinsically disordered.[20]

An interesting feature of amyloid fibrils is their rather straight geometry. As we have recently proposed,[6] such straightness of fibrils is the indication of the high stiffness and stability of amyloid fibrils, explaining their resistance to proteolysis and hence their stable existence as plaques in brains. A detailed analysis of the morphologies of various fibrils in terms of their stiffness was performed later in work of Knowles et al.,[21] showing that the stiffness of amyloid fibrils varies in a very broad range. High stiffness is attributed to the backbone hydrogen bonding modulated by side chain interactions.

PROTEIN MISFOLDING AND AGGREGATION KINETICS

The kinetics of amyloid aggregation has a specific sigmoidal shape as illustrated in Figure 1. This figure shows the time-dependent aggregation of a short fragment of Sup35 prion protein from yeast detected by thioflavin T (ThT) fluorescence assay. Aliquots were taken from the reaction mixture and mixed with ThT, the fluorescence of which increases upon binding to amyloid fibrils.[22] The lag period varies depending on the aggregation conditions. For example, it is 196 h for the aggregation experiments performed at pH 2.0 and much smaller, 11 h, if the aggregation experiment is performed at pH 5.6. For the first time, similar kinetics were observed in the earlier work of

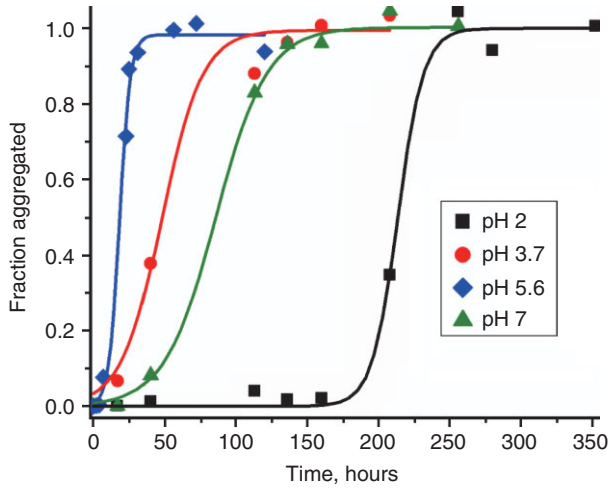

FIGURE 1 | Normalized kinetic curves of aggregation of short peptide from Sup35 yeast prion protein at various pH values: pH 7.0 (green triangles, $t_{lag} = 49$ h), pH 5.6 (blue diamonds, $t_{lag} = 11$ h), pH 3.7 (red dots, $t_{lag} = 19$ h), and pH 2.0 (black squares, $t_{lag} = 195$ h).

Hofrichter et al.,[23] in which the gelation phenomenon of purified deoxyhemoglobin was investigated. The authors proposed a model dissecting the fibril growth kinetics into two phases. The first phase is the nucleation process in which small oligomers, starting from the dimers, are formed via multiple thermodynamically unfavorable steps. During this phase, a critical oligomer of a particular size, a nucleus, is formed. The nucleus undergoes a thermodynamically favorable elongation process in which monomers are added via consecutive monomer addition steps. Application of the proposed model to the aggregation of deoxyhemoglobin led to the conclusion that the size of the nucleus for this protein is rather large, 30 monomeric units.[23] Later Jarrett and Lansbury[24] applied this model to the analysis of aggregation of amyloids. Similar to the deoxyhemoglobin gelation kinetics, the lag in the amyloid growth in this paper was attributed to the formation of nuclei or seeds. Currently, this nucleation-polymerization model is considered as a main model for the *in vitro* amyloid aggregation process. The growth of amyloid plaques *in vivo* has been investigated in a recent paper,[25] and one of the major findings is that the growth of the plaques follows an extensive lag period after which the plaques form very fast. Thus, *in vivo* and *in vitro* studies revealed a very similar pattern in the formation of amyloids—a considerably long lag period during which the formation of stable nuclei occurs. This period is considered as a key step in the entire process of the amyloid growth. However, a number of important questions arise. What are these nuclei? These are very likely oligomeric forms of the protein with lifetimes sufficient for initiating the polymerization reaction; how large are these lifetimes compared with the timescale of protein conformational dynamics? The study of aggregation of amyloids showed that the process in fact is more complex. The morphology of amyloid aggregates is not limited to fibrils. Rather, stable oligomeric samples are formed and their morphologies are different. In addition to thick fibrils, protofibrils are formed, which might be intermediates of assembly into fibrils. Finally, typical kinetic data were obtained with the use of staining of the aggregation products with fluorescent dyes such as ThT, but its binding depends on the type of aggregates. The formation of oligomers or other large morphologies of aggregates with the nonamyloid structure is not detectable by this method. As a result, the analysis of the experimental data on the amyloid aggregation is not conclusive. For example, the analysis of the early stages of the aggregation kinetics data using the approach developed by Ferrone[26] led to a conclusion that nuclei for the aggregation of poly Q peptides are monomers in particular conformations that are in equilibrium with the rest of the polyQ peptide samples.[27] At the same time, a similar theoretical model applied to the aggregation data for yeast prion sup35 protein provided the sizes for nuclei as large as hexamers for Sup35p sample, whereas the nuclei were only trimers for sup35 NMp species.[28] This controversy was analyzed in a recent paper,[29] in which the available models were critically reviewed. The major conclusion of this analysis is that ThT kinetic curves do not provide sufficient information in order to develop a mechanistic model for the aggregation process, so additional sets of experimental data such as the time dependence of the fibrils length are required. Therefore, there is a need in alternative methods allowing for the characterization of the products formed during the aggregation kinetics.

The importance in the characterization of the aggregation products of amyloid proteins is supported by the fact that fibrils are not the most toxic species, but smaller aggregates, oligomers, are toxic in *in vivo* experiments (reviewed in Refs 30–32). What are these toxic samples? Recent studies show that naturally secreted Aβ dimers and trimers at physiological concentrations induce progressive loss of hippocampal synapses.[33,34] Why small aggregates? Are these abundant species of the aggregation kinetics? Apparently, the answers require a thorough study of the aggregation kinetics, with the focus on the early stages of the process. The identification of toxic samples is a key step in the development of efficient diagnostic tools and therapeutic means for neurodegenerative disease, AD in particular. The progress in this area has been made very recently and the sections below outline these advances.

EARLY STAGES OF THE AGGREGATION KINETICS

Here, we review the results of recent studies on the early stages of amyloid aggregation, with the primary focus on the characterization of oligomeric species. Although attempts to characterize oligomeric forms of various amyloidogenic proteins have been made in various works, systematic studies have not been performed until very recently. In the paper by Bernstein et al.,[35] electrospray ionization ion-mobility mass spectrometry (ISI-MS) was used to directly characterize oligomeric species formed by amyloid-β peptides consisting of 40 and 42 amino acids, Aβ-40 and Aβ-42, respectively. Aβ-42 peptide differs from Aβ-40 by having two extra amino acids (isoleucine and alanine) at the C terminus of Aβ-40. The ISI-MS technique enables one to analyze noncovalent complexes

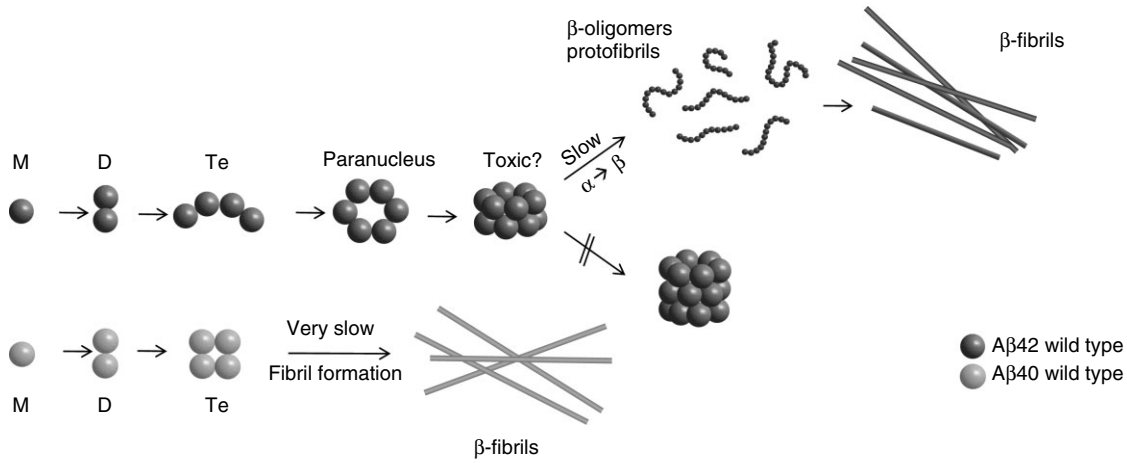

FIGURE 2 | Wild type of Aβ-40 and Aβ-42 self-assemble to form dimers and tetramers, but in further oligomerization, they have different pathways. Aβ-40 fibrillizes slowly, but directly forms a compact square shape of tetramer. On the contrary, the open type of Aβ-42 tetramers forms hexamers and dodecamers which are suggested as the primary stable intermediates for early stages of Aβ-42 aggregation. (Adapted with permission from Ref 35. Copyright 2009 Nature Publishing Group: Nature Chemistry).

persistent in the gas phase. Oligomeric species of both peptides were analyzed and these studies led to a number of new discoveries. Schematically, the aggregation pattern of Aβ-40 and Aβ-42 is shown in Figure 2. First, both peptides accumulate different types of oligomers. While dimers and tetramers were found for Aβ-40, Aβ-42 formed hexamers and dodecamers. However, the oligomers with the same number of monomer units can adopt various geometries. For example, hexamers can be linear or closed ring-type shapes. A remarkable property of the ISI-MS method is that it is capable of distinguishing such geometries. Hexamers, with closed conformations, are more compact compared with the linear oligomers and therefore have a higher mobility. As a result, a ring-type geometry was assigned to the hexamers of Aβ-42. Importantly, no species between hexamers and dodecamers, octamers for instance, can be found, suggesting that hexamers and dodecamers are the primary stable intermediates for early stages of Aβ-42 aggregation. Similar analysis of Aβ-40 sample showed that the Aβ-40 tetramers adopt compact square shape geometry. In comparison, tetramers of Aβ-42 adopt less compact species with a curved shape, enabling them to form hexameric rings upon the incorporation of a dimer. Based on these studies, a model has been proposed, according to which, assembly of Aβ-40 and Aβ-42 into fibrils follows two different pathways. At the early stages of aggregation, Aβ-40 forms dimers and tetramers. Accumulated tetramers play the role of nuclei for assembly of protofibrils. In case of Aβ-42, the hexamer is a nucleus (termed 'paranucleus') for the protofibril formation by stacking of hexameric rings. The finding on the importance of hexamers in oligomerization of Aβ-42 is in line with earlier experiments performed with the use of photochemical cross-linking of amyloid oligomers.[36] The use of various amino acid substitutions in the C-terminal region of Aβ-42 revealed the importance of hydrophobicity of C-terminus of the peptide in the paranucleus formation. However, the other parts of the peptides are far from being inert, and this issue is discussed in details in the recent review article.[37]

A combined approach utilizing several methods in the study of entire aggregation kinetics has been recently proposed.[38] In this paper, dynamic light scattering (DLS) and AFM were used to follow the aggregation process and time-resolved fluorescence of 1-anilino-8-naphthalene sulfonate and ThT to monitor conformational changes. The bovine milk lipocalin, β-lactoglobulin A (β-LGA), which forms amyloids at various conditions, was used as an experimental system. In these studies, DLS was instrumental to follow the early stages of the aggregation process. At this stage, the β-LGA monomers were converted into dimers and tetramers. The sizes of the aggregates were too small to detect them with AFM. This method was instrumental at later stages, enabling the authors to detect the formation of the globular type of oligomers, and the analysis of the AFM images led to the conclusion on the formation of oligomers with sizes between 8 and 40 monomer units. A parallel study of the protein conformation with the use of the time-resolved fluorescence indicated a conformational transition of the protein. The analysis of the AFM data revealed two aggregation pathways, with one of them leading to the formation of fibrils. Based on this set of data, the following mechanism of the

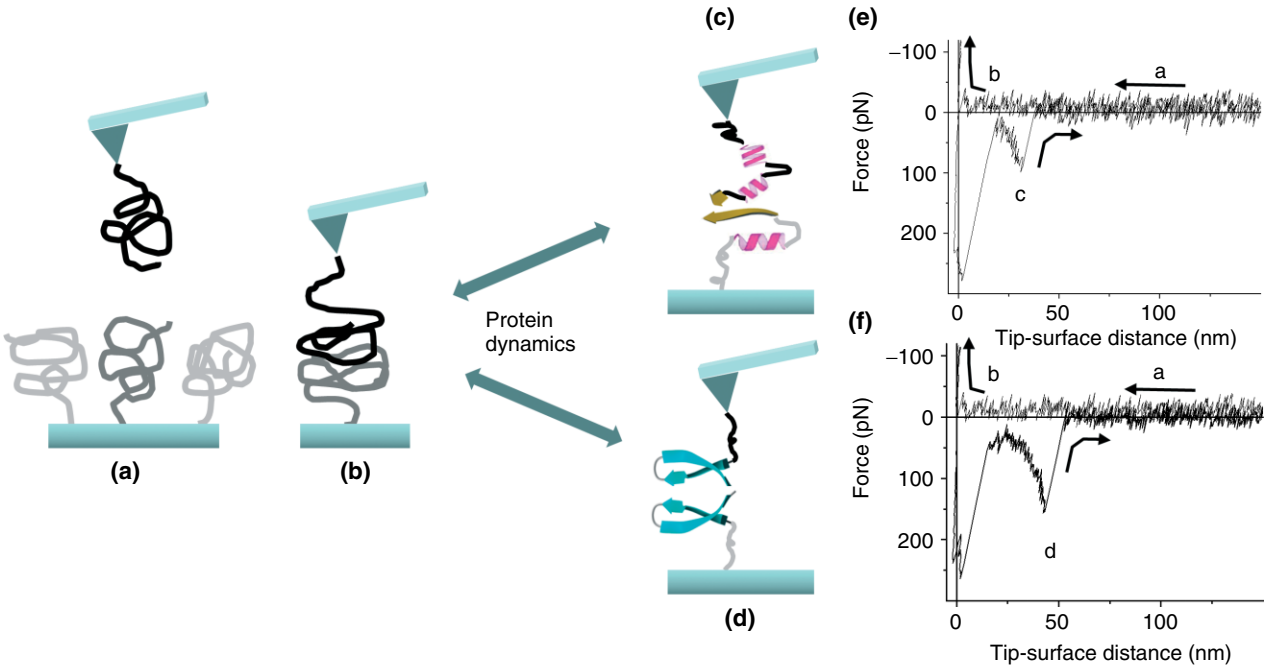

FIGURE 3 | Scheme for the atomic force microscopy (AFM) probing of misfolded interprotein interaction. The protein is tethered on the tip and on the substrate. (a) AFM tip and substrate before approaching; (b) AFM tip approaches the substrate which is capable of forming complex structure; (c) and (d) are two different complexes with low interaction forces (c) and strong interprotein interaction (d); (e) and (f) show two different force curves corresponding to scheme (c) and (d), respectively, where a and b are presented in the process of scheme (a) and (b). The peak at zero values of the tip-sample separation is originated from the nonspecific interaction between tip and substrate.

β-LGA aggregation was proposed. At the early stages of aggregation, the β-LGA monomers are converted into dimers and tetramers. Oxidation of the dimers occurs at this stage, so the tetramers are formed by incorporation of both dimeric species. These species, primarily tetramers, constitute a reservoir of intermediates used for the later stages of the aggregation process. At this stage, a critical oligomer, 16-mer, can undergo a conformational transition, leading to a conformer capable of fast and thermodynamically favorable process of fibril formation. Another state of the 16-mer slowly aggregates into nonfibrillar species.

There is a common feature in the studies performed on two different types of amyloidogenic proteins—the conversion of monomers into dimers, followed by their assembly into tetramers. No trimers are detected in both studies. This is a rather unexpected finding, as a canonical polymerization model for amyloids formation includes the formation of trimers. These findings suggest that it might be a property of dimers that makes the pathways with their accumulation preferable compared with the growth of oligomers with the use of monomers as building materials.

The answer can be provided by the analysis of the properties of dimeric forms of amyloids obtained with use of AFM force spectroscopy—a rather nontraditional method for analyzing the aggregation process recently proposed in our laboratory.[6,39] The rationale for the use of AFM force spectroscopy for the characterization of the protein misfolding and early stages of aggregation is based on a reasonable assumption that misfolded conformations of proteins differ from the folded ones by their enhanced propensity to interact with each other. Therefore, the strategy for the AFM analysis is as follows (Figure 3): Figure 3(a) shows AFM tip starting to approach the substrate. The proteins can form a complex (a dimer) upon approaching the tip to the surface (Figure 3(b)). The protein can form a complex with low interaction forces (Figure 3(c)) or adopt misfolded states to form a complex characterized by a strong interprotein interaction (Figure 3(d)). These states can be distinguished by their probing upon the retraction cycle of this method yielding different types of force curves (Figure 3(e)), as the stronger the interaction between the monomers, the higher the rupture force value. This approach was tested with the use of three different proteins, α-synuclein, lysozyme, and amyloid β peptide, using low pH as a factor inducing protein misfolding.[39] The AFM probing studies revealed the correlation between the propensity of the protein to

form aggregates and the strength of the interprotein interactions.

CHARACTERIZATION OF THE VERY EARLY MISFOLDING STAGES

Single-Molecule Force Spectroscopy

Force spectroscopy, including AFM force spectroscopy, has emerged as a powerful set of tools to follow molecular scale events capable of measuring a wide range of intermolecular interactions at single-molecule level, which is known as single-molecule force spectroscopy. This technique is widely applied to probe interactions of various types of biomacromolecules including proteins, nucleic acids, and protein–DNA complexes, to mention a few (reviewed in Refs 40–58). We will briefly describe the basics for dynamic force spectroscopy (DFS) technique, which is currently applied for a quantitative characterization of various molecular systems. The technique was introduced by Evans and Ritchie (reviewed in Ref 59), but the original model was proposed by Bell[60] almost two decades earlier for description of experiments on the cell–cell interactions. The theory for DFS has evolved since that time; different approaches for the quantitative analysis of the DFS data were proposed (see papers[61,62] and references therein), but the main idea behind DFS remains unchanged. The basics for DFS are illustrated schematically in Figure 4. In this figure, a dotted line shows the energy profile for a system that undergoes a structural transition from the ground state (G) to another state (dissociated state) (D) via a transient state (T). The first peak on the energy profile corresponds to the height of the inner barrier and the second peak corresponds to the outer barrier height. This scheme corresponds to the spontaneous dynamics of the system, but in the presence of pulling force that linearly changes with the distance, the profile changes. At a small force shown as F1 in the figure, the overall energy of the system calculated at each point is E-F1x, i.e., each point of the original energy profile is moved down by subtracting the appropriate value for F1x. This profile is shown as E-F1x curve. Both peaks remain, and most importantly the second peak corresponding to the completion of the transition is higher, although its shift down is larger than the first peak. The E-F2x graph shows a different situation. In this case, a much larger force (F2) is applied. This leads to additional deformation of the energy profile, consequently the second barrier becomes lower than the first barrier. This is an important point of the DFS, illustrating the method in case this situation, achievable experimentally, is capable of probing the

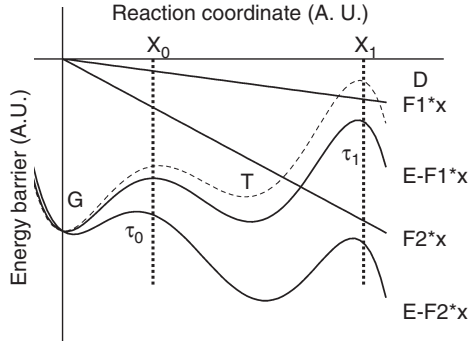

FIGURE 4 | Schematic energy landscape profile. Dotted line is the original energy profile (E-profile) in the absence of an external force. On the profile, G indicates the ground state, T the transition state, and D the dissociation state separated by potential barriers located at x_0 and x_1. External forces change the barrier heights. At small forces (F1x), the barrier at x_1 remains taller than the barrier at x_0. At large external force (F2x), the second potential barrier (x_1) becomes lower than the first potential barrier (x_0).

transient states of the system. Formally, the approach works this way. It is instructive to use Eq. 1 for the off-rate constant for forward transition reaction A → A*→D,[63] in which A is the initial ground state, A* is a transient state, and D is the dissociated state of the system corresponding to positions G, T, and D on the energy profile in Figure 4:

$$k_{\text{off}}(0) = (k_{\text{B}}T/h)\exp(-\Delta G/k_{\text{B}}T) \qquad (1)$$

where k_{B} and h are Boltzman's and Plank's constants, ΔG is free energy difference between ground state and transition state (Figure 4), and T is absolute temperature. In the presence of external force, the barriers are decreased yielding to the following equation:

$$k_{\text{off}}(F) = (k_{\text{B}}T/h)\exp[-(\Delta G - x_\beta F)/k_{\text{B}}T] \qquad (2)$$

In this equation, free energy (ΔG) is decreased by the product of the force (F) and the distance of the ground state to the activated state (the energy barrier) (x_β, $\beta = 0, 1$) along the reaction coordinate. In the range of forces at which the barrier at x_1 remains higher than the barrier x_0, extrapolation of the data to zero applied force provides the value for k_{off} (0). Similarly, performing experiments at forces exceeding the critical force value at which both barriers are equal enables one to determine the dissociation constant and the energy corresponding to the height of the inner barrier. This means that a transient state of the system can be probed at certain experimental conditions.

We now consider how (in the framework of the DFS model termed a standard model[59]) the off-rate

constant parameters, along with other characteristics of the system, can be obtained and how the profile of the energy landscape along the pulling direction can be reconstructed. In reality, the force applied to the system is not changed instantaneously, but is ramped up with a certain rate. The parameter, loading rate (ν), can be controlled experimentally. Thus, experimentally measured values and controlled parameters are rupture forces (F_R) and loading rates. The following expression linking the experimental parameters can be obtained[64]:

$$F_R = (k_B T/x_\beta)\ln[(\nu x_\beta)/(k_{off} k_B T)] \quad (3)$$

This equation shows that if experimental data for the rupture force F_R obtained at various loading rates ν are plotted against the natural logarithm of loading rate values, they will fall on a straight line from the slope and intercept of which x_β and k_{off} are determined. These values can also be used for the reconstruction of the energy landscape profile along the pulling direction. The validity of this approach was tested on numerous examples, and a few of them are related to the analysis of protein misfolding, which is discussed below. The approach also works in the case when the force-induced transition has two barriers, as shown in Figure 4. In this case, the DFS graph has two lines, enabling one to estimate the location of each barrier and their heights. We will consider these cases as well. The application of the DFS approach to protein misfolding studies requires a development of immobilization methods in order to avoid complications with nonspecific interactions. We developed a novel surface chemistry in which anchoring of protein occurs at selected primarily terminal moieties. The use of the site-specific immobilization procedure allowed us to measure the rupture of intermolecular interactions at the single-molecule level.[65] This approach was later applied to a number of different proteins and peptides, enabling us to reveal general principles of the early stages of the misfolding dependent aggregation process. The sections below briefly outline these findings.

PROBING OF THE INTERACTION OF MISFOLDED α-SYNUCLEIN, PRION PROTEIN, AND Aβ

α-Synuclein—Structure and Function

There are numerous lines of evidence proving that the misfolding and aggregation of α-synuclein are the pathological hallmarks of several neurodegenerative disorders, including Parkinson's disease, the Lewy body variant of AD, dementia with Lewy bodies, multiple system atrophy, and neurodegeneration with brain iron accumulation type 1.[1,66,67] First, α-synuclein is a major fibrillar component of Lewy bodies (inclusions present in brain regions that are functionally damaged in PD).[68] Second, three mutations in the α-synuclein gene (A30P, E46K, and A53P) are linked to the early-onset familial PD.[69–71] Third, the overexpression of α-synuclein in both mice and Drosophila has been shown to lead to PD-like phenotypes consisting of motor deficits and neuronal loss.[72,73] Fourth, the aggregated forms of α-synuclein are inducers of cellular stress and activators of immunity in neurodegenerative diseases and affect neuronal dysfunction and loss.[74,75]

α-Synuclein, which is abundantly expressed in neurons, localized in presynaptic nerve terminals, belongs to a family of natively unfolded proteins and lacks a stable tertiary structure at physiological conditions. Human α-synuclein is a 140-amino acid protein, which has three distinct regions: N-terminal region (1–60), which contains 11-amino acid imperfect repeats (coding for amphipathic helices) with a consensus motif (KTKEGV), the central region (61–95), which contains a highly amyloidogenic NAC (non-Aβ component of AD amyloid) region followed by two additional repeats, and the C-terminal region (96–140), which is rich in acidic residues and prolines, suggested to adopt a disordered conformation. Because α-synuclein is random-coiled in aqueous solution, it is hard to detect its structure directly. In a micelle-bound state or in amyloid fibrils, α-synuclein adopts ordered structures such as α-helical or β-sheet structure. It was shown that the membrane interaction is mediated by major conformational changes within the 11 amino acid repeats in the N-terminal region.[76] The structure of micelle-bound α-synuclein has been determined by solution state NMR,[77] which showed that Val3-Val37 and Lys45-Thr92 form curved α-helices, connected by a linker in an antiparallel arrangement, followed by a short region of Gly93-Lys97 and then by a highly mobile tail of Asp98-Ala140. The structure is schematically shown in Figure 5(a). In addition to the α-synuclein structure in membrane-bound state, there have been many studies on the structure of α-synuclein in amyloid fibrils. Residues 71–82, which are in the middle of the hydrophobic domain of human α-synuclein, are shown to be necessary and sufficient for α-synuclein fibrillization.[78] A high-resolution SS-NMR study on full-length α-synuclein fibrils illustrated that the region of residues V38-V95 is a β-strand-rich core region.[79] There are at least two distinct fibril nucleation mechanisms that exist for α-synuclein fibril formation, which

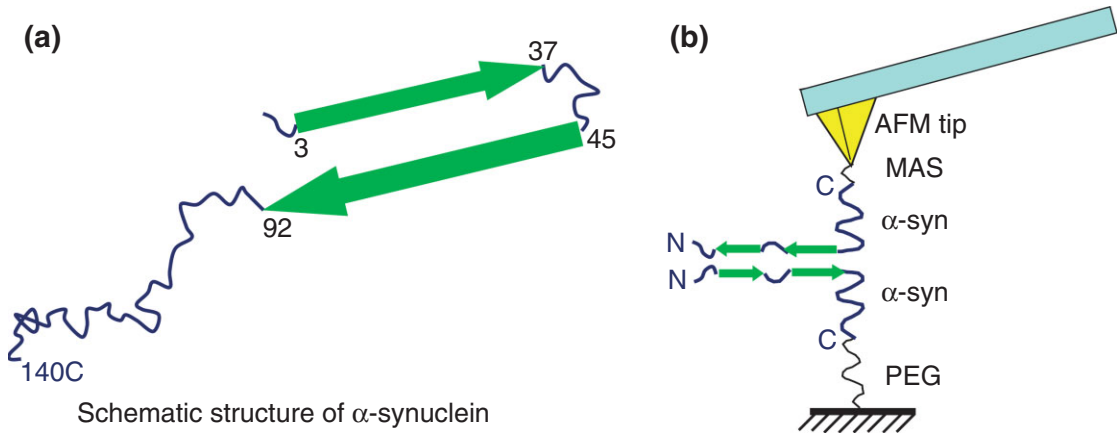

FIGURE 5 | Atomic force microscopy (AFM) experimental setup to probe the interaction between α-synuclein monomers. Scheme (a) schematically shows the α-synuclein structure within micelles and (b) illustrates the immobilization of the surfaces. α-Synuclein was attached to the MAS functionalized AFM tip (top) by covalent bonds with Cys moiety of the protein. The mica surface (bottom) was functionalized with polyethylene glycol (PEG) treated with amynopropylsilatrane (APS-mica, see Refs 64,65) surface.

proved the polymorphisms of α-synuclein fibrils. In α-synuclein fibrils, a partially folded intermediate was found,[80] and low pH or high temperature facilitates the partially folded conformational formation, which is correlated to the enhanced formation of α-synuclein fibrils.

Molecular Mechanisms of α-Synuclein Misfolding and Aggregation

AFM and EM have shown the variety of α-synuclein morphologies and provided the information of the secondary structure of α-synuclein,[6,81–83] but very little is currently known about the molecular mechanism underlying α-synuclein misfolding and aggregation such as how α-synuclein misfolds, why the misfolded conformation of the protein is formed, and how the misfolded protein forms various morphological aggregates. Importantly, the conformation of misfolded protein prior to aggregation needs to be identified. Factors that lead to protein misfolding and aggregation *in vitro* are poorly understood, not to mention the complexities involved in the formation of protein nanoassemblies with different morphologies. Although it is well known that the same protein under pathological conditions can lead to the formation of fibrillar, pore-like, spherical, or amorphous aggregates with diverse biological consequences, the conditions leading to misfolding and formation of such abnormal complexes are unclear, let alone their prevention. A better understanding of the molecular mechanisms of misfolding and aggregation will facilitate rational approaches to prevent protein misfolding leading to aggregation. Very likely, there are a number of such noncanonical protein conformations that exist transiently and which transform from one into another. Several methods have been utilized for the study of the molecular mechanisms of α-synuclein misfolding and aggregation. One of them is molecular dynamics (MD) simulation, which has been used to clarify the molecular mechanisms of α-synuclein aggregation. Using this method, it was concluded that α-synuclein homodimers are formed on the membrane and incorporate additional α-synuclein molecules to form ring-like structures of pentamers or hexamers.[84,85] Fluorescence microscopy, along with fluorescence resonance energy transfer,[86,87] are other methods by which the oligomeric intermediates in α-synuclein fibrillation were characterized.[88]

α-Synuclein Misfolding and Interaction—DFS Analysis

To probe the interaction of misfolded α-synuclein with AFM,[89,90] the monomers of α-synuclein were immobilized on the AFM probe and the substrate at the C-terminus of the protein (Figure 5(b)). In these experiments, α-synuclein mutant, in which Ala140 was replaced with cysteine, enabled us to perform specific immobilization using a thiol chemistry.[65] The AFM force experiments produce force curves similar to one shown in Figure 6(a). The rupture peak appears at a certain distance on the force curve, corresponding to the extension of the linker, and a segment of α-synuclein not involved into the complex formation. The use of the linker with the length ca 30 nm enabled us to move the specific rupture event far from the short-distance nonspecific interactions that typically appear in the AFM experiments. Such force curves were obtained by multiple probing of different

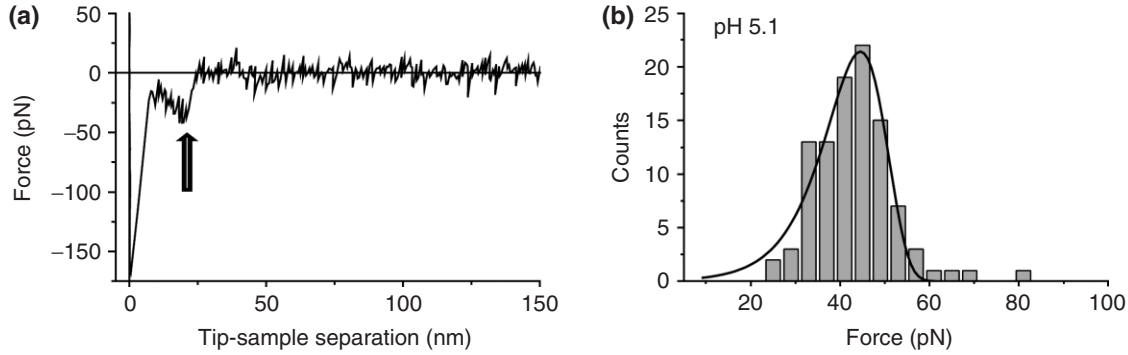

FIGURE 6 | Probing of the interaction between α-synuclein molecules. Scheme (a) shows a representative force curve between α-synuclein molecules at pH 5.1. The rupture event is indicated with an arrow. Plate (b) shows the rupture force distribution histogram obtained for multiple experiments performed at pH 5.1 at apparent loading rate 3953 pN/s. The solid line is the fit of the experimental data with the probability density function distribution, which provides the maximal rupture force 44.6 ± 1.2 pN.

immobilized proteins using the same loading rate value. A complete data set typically contained several hundred rupture events, and Figure 6(b) shows the results of such multiple measurements assembled as a histogram. Typically, such a set is analyzed using the probability function distribution. The most probable rupture force is located at the maximum of the distribution[91,92] and this maximum is used as a data point for plotting the DFS spectrum, corresponding to a selected loading rate.[89,90] To generate the DFS spectrum, probing of protein–protein interaction is performed in a range of approach-pulling rates, and the results of such analysis are plotted in a semi-logarithmic plot corresponding to probing of α-synuclein interaction at pH 5.1 is shown in Figure 7(a). The plot is linear, suggesting that the complex dissociation follows a simple one-barrier path. Using Eq. 3, from this plot, we obtained the values for k_{off} and x_β. The profile of the energy landscape for these conditions obtained with these values is shown in Figure 7(b). As we described above, it is a one-barrier path with the energy barrier of 16.6 kcal/mol (or 28.1 k_BT). Note that the complex formed by two α-synuclein monomers is rather stable, having the lifetime ca 0.27 s. The barrier height obtained in this analysis is consistent with the dynamics of other systems studied with the force spectroscopy.[63]

Figure 8 shows the DFS data obtained at pH 3.7. The DFS semi-log plot is shown in Figure 8(a), and it is approximated with two lines, suggesting that the dissociation of the same protein at different pHs follows a different path. The profile calculated using the values for k_{off} and x_β for low-applied force and high-applied force regimes are shown in Figure 8(b). The difference of the inner and outer barriers is more than 4 k_BT, enabling us to probe the two barriers separately. Interestingly, the outer

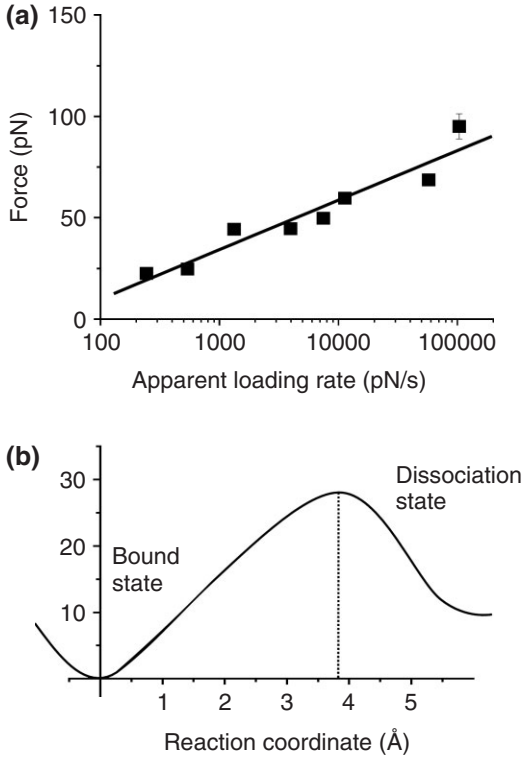

FIGURE 7 | (a) The dynamic force spectroscopy plot for the atomic force microscopy probing of α-synuclein interaction measured at pH 5.1 The lifetime for the dimer dissociation is 0.27 s. (b) The profile of the energy landscape for the α-synuclein dimer dissociation at pH 5.1. It shows a one-barrier energy path. The energy barrier height is 28.1 k_BT.

barrier provides the off-rate constant close to the one obtained in experiments at pH 5.1, giving the lifetime for the complex ca 1.35 s. The dissociation via the inner barrier is a much more dynamic process, so the transient state lives ca 50 ms. A number of important conclusions have emerged from these studies which

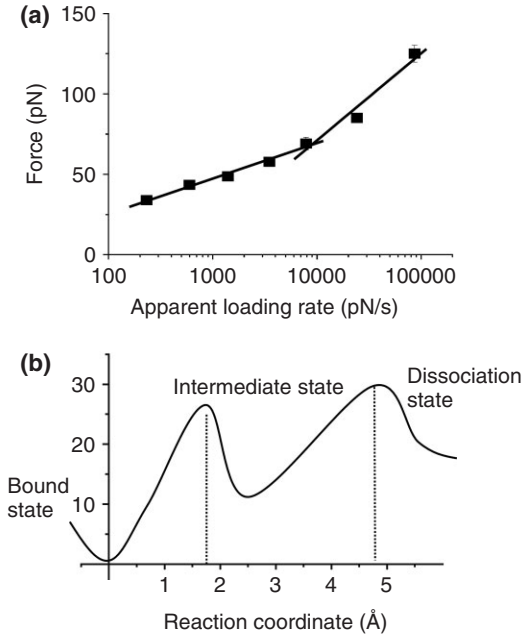

FIGURE 8 | (a) The dynamic force spectroscopy plot for the atomic force microscopy probing of α-synuclein interaction measured at pH 3.7. (b) The corresponding energy landscape profile for the α-synuclein dimer dissociation at pH 3.7. The heights of energy for the inner and outer barriers are 26.4 and 29.8 $k_B T$, respectively. The lifetimes for the two states of the dimer (outer and inner barriers) are 1.35 s and 50 ms, respectively.

are discussed in the last section of the paper along with the data obtained for other misfolding systems.

Misfolding and Interactions between Short Peptides from Sup35 Yeast Prion Protein

Several diseases are linked to misfolding and aggregation of prion proteins. For example, Creutzfeldt–Jacob disease, kuru, and Gerstmann–Straussler–Scheinker syndrome are categorized as prion diseases. In prion diseases, the infectious particles are proteins that propagate by transmitting a misfolded state of a protein, leading to the formation of aggregates and ultimately to neurodegeneration.

The aggregation of proteins is a complex process which proceeds via many intermediate states that include oligomers, strings of oligomers (protofibrils), and fibrils. Although it is believed that the infectious form of prions is the self-propagating fibrillar or amyloid PrP protein,[93] there is increasing evidence that the end-product of aggregation—the formation of fibrils and big aggregates—is not the main cause of the disease state. There is uncertainty about which species in this complex aggregation pathway are responsible for toxicity. Although the infectivity of prions is associated with a wide range of aggregated states, small oligomers of aggregated prion proteins have been suggested to be minimally infectious particles. A recent study revealed that infectivity of PrP is the greatest for particles 17–27 nm in size, corresponding to 300–600 kDa.[94] These oligomeric particles should consist of 14–28 prion monomers. The infectivity is decreased for larger aggregates and virtually absent for oligomeric fractions of less than five molecules.[94]

This accumulating evidence highlights the importance of accessing the very early steps in the aggregation process in order to understand the mechanism of aggregation. Characterization of these steps with conventional, ensemble-based methods is challenging due to the dynamic and transient nature of early aggregation stages. Single-molecule methods can provide unique information on the structure, energetics, and dynamics of intermediate transient species. Among these methods are approaches for single-molecule probing, including AFM (Figure 3). Although this probing approach involves two molecules, it is reasonable to refer to this method as a single-molecule method, as it deals with interactions of individual molecules with no interference from other molecules. The most attractive feature of single-molecule experiments is that these experiments are able to analyze the transient states by their propensity to interact with each other. Using such probing approach, one is able to identify the states characterized by elevated intermolecular interactions, i.e., candidates for misfolded states. Misfolded, aggregation-prone conformations of a protein molecule differ from other conformations by their increased propensity to associate with each other, promoting formation of nanoaggregates.[65] A monomeric protein molecule should undergo structural reorganization in order to adopt intermediate conformational states (misfolded conformations) required for the initiation of aggregation.[95] Interactions between misfolded proteins facilitate the very first step in the aggregation process—the formation of the dimer. The subpopulation of misfolded states can be very small. For example, aggregation of HypF-N is initiated by a population of partially folded conformations, which exist in equilibrium with native state, and comprises less than 1%.[96] Another example is single-molecule studies of conformational equilibria of monomeric α-synuclein.[97,98] These studies found that a subpopulation of strongly interacting molecules comprises only 6% of total conformational space for wild type α-synuclein and such population increases under conditions that promote aggregation of α-synuclein. The propensity for conformational

transitions could be modulated by primary sequence or external factors such as environmental conditions, interactions with other proteins, toxins, cellular components, and/or cellular membrane.

We have used force spectroscopy approach to measure interactions between individual molecules of short peptide CGNNQQNY with a cysteine incorporated to facilitate immobilization for force spectroscopy. This peptide is a part of yeast prion protein Sup35 and was found to be amyloidogenic, seeding aggregation of the entire protein.[99] The aggregation of this peptide results in aggregates of fibrillar morphology in a range of environmental conditions. The kinetic profiles of fibril formation tested with ThT fluorescence at different pH values of solution are shown in Figure 1. The aggregation kinetics is the fastest at pH 5.6, which is close to the pI value of the peptide (5.3). We have chosen this pH value for the measurements of interactions between individual peptides. The peptide monomers were attached to AFM tip and mica surface in the same manner as described above for α-synuclein.[64,65] The rupture events observed in force spectroscopy measurements were analyzed in a similar way as described above for α-synuclein. The DFS plot obtained for interactions of CGNNQQNY peptide at pH 5.6 is shown in Figure 9(a). The plot has distinct low- and high-force parts. Probing at high loading rates (large forces) is characterized by a very steep linear plot, producing the off-rate dissociation constant as high as 147 s^{-1}. Compared with this value, the low-force dissociation range is much less dynamic, $k_{off} = 1.8\ s^{-1}$. Dissociation of intermolecular contact that involves overcoming of more than one activation barrier results in a dynamic force spectrum with several distinguishable regimes characterized by different slopes.[100] Two slopes of DFS plot are translated into two activation energy barriers for dissociation of peptide dimeric contact. The corresponding energy profile is shown in Figure 9(b).

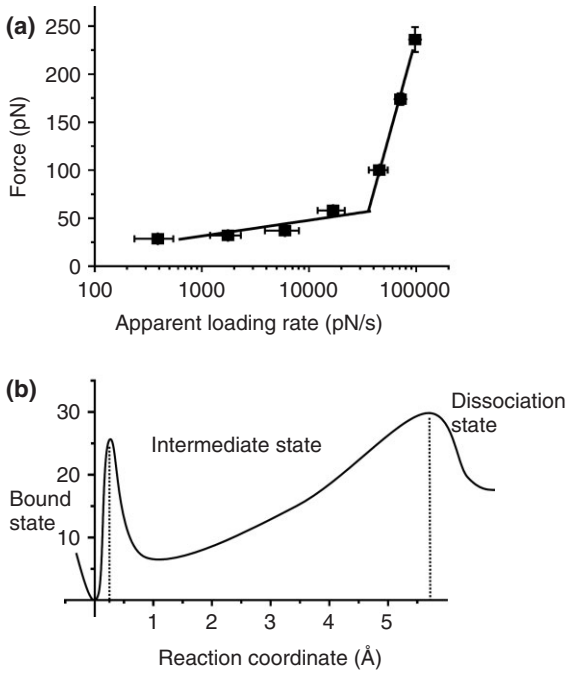

FIGURE 9 | Dynamic force spectroscopy (DFS) analysis of CGNNQQNY interactions measured at pH 5.6. (a) DFS plot and (b) schematic profile of energy landscape for dissociation of CGNNQQNY dimer at pH 5.6, where the first barrier is located at ~0.2 Å with 24.5 k_BT of energy barrier and the second barrier is at ~5.7 Å with 28.9 k_BT.

Misfolding and Interactions between Aβ Peptides

AD, characterized by the deposition of insoluble aggregates of fibrillar Aβ protein, has been studied as the most popular subject of neuronal disease. However, there is growing evidence showing that the soluble Aβ oligomers are potentially synaptotoxic species.[101,102] Recently, the initial stage of Aβ aggregation has been studied using various methods, suggesting that the oligomerization pathway between Aβ-40 and Aβ-42 is different after forming dimers[35] and their oligomers have different conformational structure from fibrils, which are related to structure–neurotoxic activity.[4,103,104] Also, Aβ undergoes conformational changes from largely unstructured or α-helical to higher β-sheet content, depending on environmental conditions, while self-assembling.[4,105–107] However, the mechanism of how to initiate the misfolding and aggregation of Aβ is still unclear.

We performed AFM of Aβ-40 following the above described methodology,[89] using essentially the same immobilization procedure for the peptide. The peptide was synthesized with cysteine placed at the N-terminal position. The rationale for the use of N-terminus for the immobilization stems from the known fact that N-terminal part of Aβ-40 is not directly involved in the aggregation process.[108,109] The results of the DFS analysis for the experiments performed at two pH values, pH 2.7 and 5, are shown in Figure 10. At both pH values, the DFS results showed two linear approximations, suggesting that the dissociation process is a two-step transition (Figure 10(a) and 10(b)). The corresponding energy profiles are shown in Figure 10(c) and (d), respectively. The similarities of energy profiles are the large differences in the off-rate constants for low- and high-force regimes, respectively. They correspond to the lifetimes for

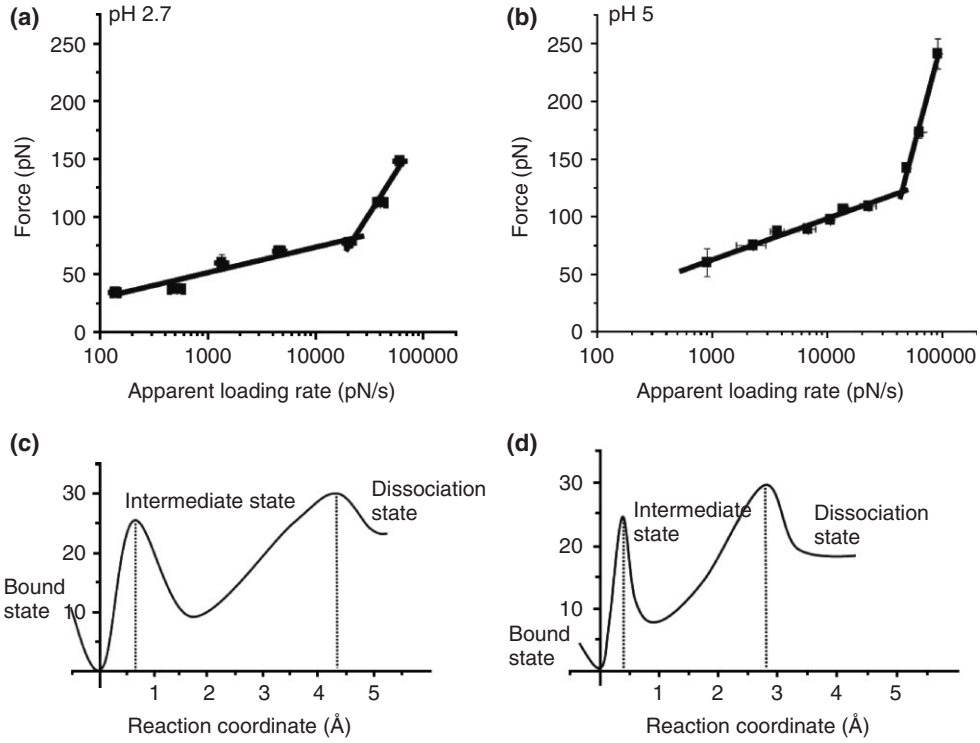

FIGURE 10 | The dynamic force spectroscopy (DFS) plot and energy landscape profile probing of Aβ-40 interaction. Plates (a) and (b) show the DFS plot measured at pH 2.7 and 5.0, respectively. The corresponding energy profiles are shown in (c) (pH 2.7) and (d) (pH 5.0). The energy profiles show two barriers at $x_0 \sim 0.6$ Å with 24.8 k_BT and $x_1 \sim 4.3$ Å with 30.3 k_BT at pH 2.7 and at $x_0 \sim 0.3$ Å with 24.7 k_BT and $x_1 \sim 2.7$ Å with 29.5 k_BT at pH 5.0. The lifetime at each transition state was ~10 ms and ~2.7 s at pH 2.7 and ~9 ms and ~1.1 s at pH 5.0, respectively.

transient states (inner barriers are obtained from the high loading rates) in the range of 1–10 ms, whereas outer barrier is much higher. Therefore, the path from the ground state to full dissociation is characterized by significantly longer lifetimes, 1–4 s. The difference between the data obtained at these conditions are the positions of outer peaks that are located at larger distance ($x_\beta \sim 4.3$ Å) for the pH 2.7 conditions compared with the peak position at pH 5 ($x_\beta \sim 2.7$ Å), indicating the difference in the conformation of Aβ-40 at these conditions. We have also shown very recently (Kim et al, in preparation) that the number of events drops if the measurements are performed at pH 7, which is consistent with previous data.[39] In addition, DFS analysis revealed an approximately 10-fold decrease of the dimer's lifetime compared with the lifetime obtained at pH 2.7.

PROTEIN MISFOLDING, INTERACTION, AND EARLY STAGES OF AGGREGATION

There are a number of important conclusions emerging from the DFS analysis of the different systems described above. One of them is the lifetime of misfolded dimeric complexes—this parameter is within the range of a second. It is instructive to discuss these numbers along the line of the protein dynamics schematically shown in Figure 11. Each protein is a dynamic system capable of adopting various transient states, along with the most stable native state, termed here a 'folded monomer'. Transient states, including fully unfolded and misfolded states, are shown in the scheme. Depending on the scale of the dynamics, the timescale of local protein dynamics is in the range of nanoseconds and large-scale dynamics may occur in the microsecond time scale.[110] Computer-based MD approach is widely applied to the analysis of protein dynamics, with the focus on the protein misfolding and substantial conformational changes. These are analyzed with respect to the fact that the protein misfolding occurs in the time scale of nanoseconds (paper[95] and references therein). Therefore, we indicate the range of 10 ns to 1 μs (10^{-6} s) as a time scale for the protein dynamics that involve the formation of misfolded conformations. When two dynamic misfolded proteins interact to form a dimer, the system can live as long as a second. Compared with the dynamics of monomeric proteins, the misfolded conformation of the protein in the dimeric state is 10^6 times more stable. This is a very important finding, suggesting that the formation of dimers leads to enormous stabilization of the protein misfolded state; in other words, dimerization is the mechanism by which a misfolded state of the protein is stabilized. The high stability of dimers means that the probability of the aggregation steps with participation of dimers is 10^6 times higher compared with a reaction without them. For example, the

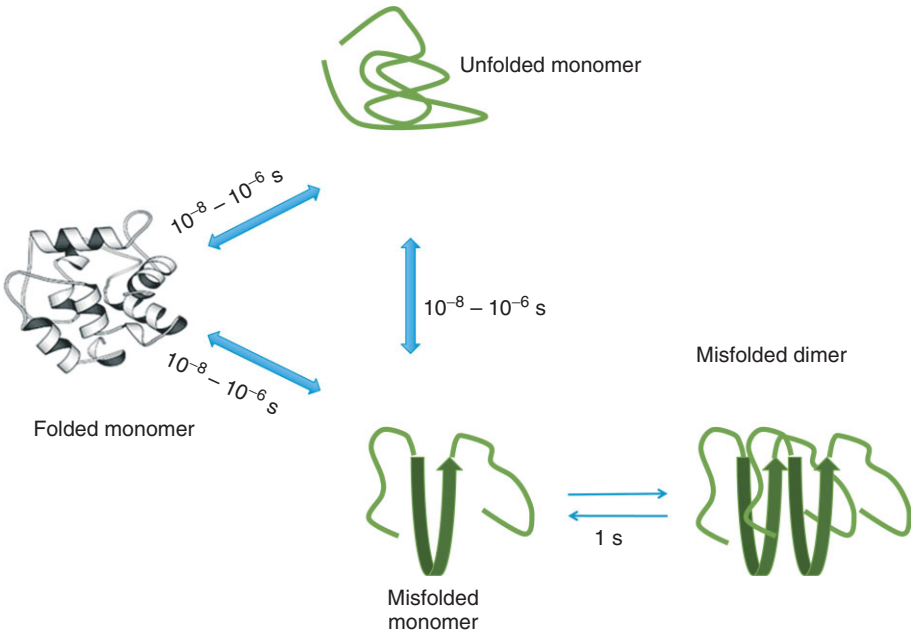

FIGURE 11 | A schematic representation of the protein dynamics. The transitions of the folded (native) state of the protein to unfolded and misfolded states are shown for the simplicity only. Characteristic times for the transition between these states as well as the dimer lifetime are shown above the arrows.

probability of tetramer formation with the assembly of two dimers will be 10^6 times higher compared with the formation of trimers via the interaction of dimer and monomer. Earlier, we mentioned a recent publication in which Aβ peptide oligomers with only even numbers of monomers are formed.[35] High stability of the dimers provides the explanation of these findings. The difference of the protein state between the monomeric and dimeric forms has further support from another recent publication.[4] In this paper, the dimers of Aβ peptides along with other oligomeric forms were photocross-linked, isolated from the gel, and the resulting structures were analyzed by CD spectroscopy. A dramatic change of the peptide conformation within the dimers compared with the monomeric states was found in this paper. There were also changes between other oligomers, but these were comparatively minor changes. Another recent publication[101] analyzed dimers of Aβ peptides isolated from brain. It was found that dimers are abundant species isolated from the brain and they have a high neurotoxicity. Recent studies show that naturally secreted Aβ dimers and trimers induce progressive loss of hippocampal synapses.[33,34] It has been recently discussed that oxidation is able to stabilize the dimers *in vitro* as well as within the cell.[38]

Thus, our data appear to confirm the hypothesis that dimers play a key role in the aggregation process. According to our model, the formation of dimers is a mechanism by which a misfolded state of the protein is stabilized to a significant extent. Due to a long lifetime, the probability of further interactions involving dimers dramatically increases. Therefore, the ability to form long lifetime dimers is a fundamental property of the misfolded states of the protein, and this dimer formation triggers the protein aggregation process. The described model is a paradigm shift of the protein misfolding and aggregation phenomenon, pointing to a critical role of misfolded dimer formation in this process. Importantly, the proposed model poses dimers as appropriate targets in the development of the treatments for protein misfolding diseases. The search of efficient diagnostics should be focused on the detection of dimers, a large concentration of which will trigger a rapid aggregation process. The dimers should be targets in the development of efficient preventions, so finding the means for their dissociation would be a straightforward approach in this direction. AFM is a very useful approach in the search of appropriate candidates, as the destabilization effect of a potential compound can be characterized quantitatively. Although the dimers are stable enough to shift the conformation equilibrium of the protein conformational dynamics to the aggregation pathway, higher oligomers such as trimers, tetramers, and so on would be also important for the aggregate growth, and their property should be characterized in order to get a complete picture of the process. The DFS studies of various oligomers can help identify species (nuclei) that are responsible for the fast growth of fibrils. According to recent publications,[111–113] conformational transitions within such nuclei are required for triggering the fibrillation step and these transitions are dependent on the oligomer size.

The DFS data and the energy profile show that the dynamics of dimers is rather complex. The energy profile has two barriers, resulting in two types of dimeric forms of the protein with different lifetimes. The difference varied between 10- and 100-fold, so the shortest lifetime in the range of 10 ms is also much longer compared with the characteristic times for the dynamics of the monomers. One of the assumptions is that these two states result in different aggregation pathways of the protein. We proposed this aggregation model earlier,[6] and the recent data indirectly support this view. It is known that oligomeric forms have different morphologies. Along with spherical particles, small particles with toroidal shape (annular aggregates) are also formed (e.g., papers[6,37] and references therein). According to the recent model for the aggregation of Aβ peptides described in paper,[37] oligomer formation pathways are different from the fibril formation pathway that occurs rapidly when small oligomeric paranuclei are formed. It is tempting to assign different transient states for the dimers detected in the DFS experiments as the initial states for originating two different aggregation pathways. We did not discuss the process of the transition of natively folded protein to misfolded states. It is typically considered that the formation of an intrinsically disordered state is the first step prior to misfolding.[6] However, there are examples indicating that it may not be a general rule. For example, transthyretin is natively tetrameric protein, and its aggregation into amyloids starts with the tetramer dissociation.[114]

In conclusion, the application of nanoimaging and nanoprobing methods to the phenomenon of the protein self-assembly into aggregates was very fruitful. AFM imaging was very instrumental for detecting nanoaggregates of different morphologies. A big splash was made by observations of annular particles, due to their similarity with membrane pores[115] imaged with AFM earlier in the group of R. Lal.[116] Importantly, these pore-like structures were formed after reconstitution of the planar lipid bilayer in the presence of Aβ peptide and showed the ion conductivity properties of doing so. Later works from the same group revealed a number of interesting properties of the Aβ channels.[117–120] The use of another AFM modality, the capability to measure intermolecular interactions, opened new prospects for nanoprobing techniques in applications to the protein misfolding and aggregation field. We believe that future advances in both methods will be more productive and shed a new light in our understanding the details of the protein misfolding and aggregation process.

ACKNOWLEDGEMENTS

The authors thank L. Shlyakhtenko for critical reading of the manuscript and comments, A. Portillo for reading and editing of the text, and other lab members for useful discussion of the results. Grant sponsors: DOE (DE-FG02-08ER64579), NATO (CBN.NR.NRSFP 983204), and NSF (EPS-0701892) (to YLL).

REFERENCES

1. Dobson CM. Principles of protein folding, misfolding and aggregation. *Semin Cell Dev Biol* 2004, 15: 3–16.

2. Madine J, Jack E, Stockley PG, Radford SE, Serpell LC, Middleton DA. Structural insights into the polymorphism of amyloid-like fibrils formed by region 20–29 of amylin revealed by solid-state NMR and X-ray fiber diffraction. *J Am Chem Soc* 2008, 130:14990–15001.

3. Schmidt M, Sachse C, Richter W, Xu C, Fandrich M, Grigorieff N. Comparison of Alzheimer Abeta(1–40) and Abeta(1–42) amyloid fibrils reveals similar protofilament structures. *Proc Natl Acad Sci U S A* 2009, 106:19813–19818.

4. Ono K, Condron MM, Teplow DB. Structure-neurotoxicity relationships of amyloid beta-protein oligomers. *Proc Natl Acad Sci U S A* 2009, 106:14745–14750.

5. Maurstad G, Prass M, Serpell LC, Sikorski P. Dehydration stability of amyloid fibrils studied by AFM. *Eur Biophys J* 2009, 38:1135–1140.

6. Lyubchenko YL, Sherman S, Shlyakhtenko LS, Uversky VN. Nanoimaging for protein misfolding and related diseases. *J Cell Biochem* 2006, 99:53–70.

7. Fernandez-Busquets X, de Groot NS, Fernandez D, Ventura S. Recent structural and computational insights into conformational diseases. *Curr Med Chem* 2008, 15:1336–1349.

8. Munishkina LA, Fink AL. Fluorescence as a method to reveal structures and membrane-interactions of amyloidogenic proteins. *Biochim Biophys Acta* 2007, 1768:1862–1885.

9. Perutz MF, Finch JT, Berriman J, Lesk A. Amyloid fibers are water-filled nanotubes. *Proc Natl Acad Sci U S A* 2002, 99:5591–5595.
10. Perutz MF, Pope BJ, Owen D, Wanker EE, Scherzinger E. Aggregation of proteins with expanded glutamine and alanine repeats of the glutamine-rich and asparagine-rich domains of Sup35 and of the amyloid beta-peptide of amyloid plaques. *Proc Natl Acad Sci U S A* 2002, 99:5596–5600.
11. Sawaya MR, Sambashivan S, Nelson R, Ivanova MI, Sievers SA, Apostol MI, Thompson MJ, Balbirnie M, Wiltzius JJ, McFarlane HT, et al. Atomic structures of amyloid cross-beta spines reveal varied steric zippers. *Nature* 2007, 447:453–457.
12. Lynn DG, Meredith SC. Review: model peptides and the physicochemical approach to beta-amyloids. *J Struct Biol* 2000, 130:153–173.
13. Petkova AT, Ishii Y, Balbach JJ, Antzutkin ON, Leapman RD, Delaglio F, Tycko R. A structural model for Alzheimer's beta-amyloid fibrils based on experimental constraints from solid state NMR. *Proc Natl Acad Sci U S A* 2002, 99:16742–16747.
14. Balbach JJ, Petkova AT, Oyler NA, Antzutkin ON, Gordon DJ, Meredith SC, Tycko R. Supramolecular structure in full-length Alzheimer's beta-amyloid fibrils: evidence for a parallel beta-sheet organization from solid-state nuclear magnetic resonance. *Biophys J* 2002, 83:1205–1216.
15. Petkova AT, Buntkowsky G, Dyda F, Leapman RD, Yau WM, Tycko R. Solid state NMR reveals a pH-dependent antiparallel beta-sheet registry in fibrils formed by a beta-amyloid peptide. *J Mol Biol* 2004, 335:247–260.
16. Baxa U, Wickner RB, Steven AC, Anderson DE, Marekov LN, Yau WM, Tycko R. Characterization of beta-sheet structure in Ure2p1-89 yeast prion fibrils by solid-state nuclear magnetic resonance. *Biochemistry* 2007, 46(45):13149–13162.
17. Chan JC, Oyler NA, Yau WM, Tycko R. Parallel beta-sheets and polar zippers in amyloid fibrils formed by residues 10–39 of the yeast prion protein Ure2p. *Biochemistry* 2005, 44:10669–10680.
18. Shewmaker F, Wickner RB, Tycko R. Amyloid of the prion domain of Sup35p has an in-register parallel beta-sheet structure. *Proc Natl Acad Sci U S A* 2006, 103:19754–19759.
19. Wickner RB, Dyda F, Tycko R. Amyloid of Rnq1p, the basis of the [PIN+] prion, has a parallel in-register beta-sheet structure. *Proc Natl Acad Sci U S A* 2008, 105:2403–2408.
20. Tompa P. Structural disorder in amyloid fibrils: its implication in dynamic interactions of proteins. *FEBS J* 2009, 276:5406–5415.
21. Knowles TP, Fitzpatrick AW, Meehan S, Mott HR, Vendruscolo M, Dobson CM, Welland ME. Role of intermolecular forces in defining material properties of protein nanofibrils. *Science* 2007, 318:1900–1903.
22. LeVine H, III. Thioflavine T interaction with synthetic Alzheimer's disease beta-amyloid peptides: detection of amyloid aggregation in solution. *Protein Sci* 1993, 2:404–410.
23. Hofrichter J, Ross PD, Eaton WA. Kinetics and mechanism of deoxyhemoglobin S gelation: a new approach to understanding sickle cell disease. *Proc Natl Acad Sci U S A* 1974, 71:4864–4868.
24. Jarrett JT, Lansbury PT Jr. Seeding "one-dimensional crystallization" of amyloid: a pathogenic mechanism in Alzheimer's disease and scrapie? *Cell* 1993, 73:1055–1058.
25. Meyer-Luehmann M, Spires-Jones TL, Prada C, Garcia-Alloza M, de Calignon A, Rozkalne A, Koenigsknecht-Talboo J, Holtzman DM, Bacskai BJ, Hyman BT. Rapid appearance and local toxicity of amyloid-beta plaques in a mouse model of Alzheimer's disease. *Nature* 2008, 451:720–724.
26. Ferrone F. Analysis of protein aggregation kinetics. *Methods Enzymol* 1999, 309:256–274.
27. Chen S, Ferrone FA, Wetzel R. Huntington's disease age-of-onset linked to polyglutamine aggregation nucleation. *Proc Natl Acad Sci U S A* 2002, 99:11884–11889.
28. Krzewska J, Tanaka M, Burston SG, Melki R. Biochemical and functional analysis of the assembly of full-length Sup35p and its prion-forming domain. *J Biol Chem* 2007, 282:1679–1686.
29. Bernacki JP, Murphy RM. Model discrimination and mechanistic interpretation of kinetic data in protein aggregation studies. *Biophys J* 2009, 96:2871–2887.
30. Yankner BA, Lu T. Amyloid beta-protein toxicity and the pathogenesis of Alzheimer disease. *J Biol Chem* 2009, 284:4755–4759.
31. Li S, Shankar GM, Selkoe DJ. How do soluble oligomers of amyloid beta-protein impair hippocampal synaptic plasticity? *Front Cell Neurosci* 2010, 4:5.
32. Li S, Hong S, Shepardson NE, Walsh DM, Shankar GM, Selkoe DJ. Soluble oligomers of amyloid beta protein facilitate hippocampal long-term depression by disrupting neuronal glutamate uptake. *Neuron* 2009, 62:788–801.
33. Shankar GM, Bloodgood BL, Townsend M, Walsh DM, Selkoe DJ, Sabatini BL. Natural oligomers of the Alzheimer amyloid-beta protein induce reversible synapse loss by modulating an NMDA-type glutamate receptor-dependent signaling pathway. *J Neurosci* 2007, 27:2866–2875.
34. Yankner BA, Lu T, Loerch P. The aging brain. *Annu Rev Pathol* 2008, 3:41–66.
35. Bernstein SL, Nicholas F. Dupuis, Noel D. Lazo, Thomas Wyttenbach, Margaret M. Condron, Gal Bitan, David B. Teplow, Joan-Emma Shea, Brandon T.

Ruotolo, Carol V. Robinson, et al. Amyloid-b protein oligomerization and the importance of tetramers and dodecamers in the aetiology of Alzheimer's disease. *Nature Chemistry* 2009, 1:326–331.

36. Bitan G, Teplow DB. Rapid photochemical cross-linking—a new tool for studies of metastable, amyloidogenic protein assemblies. *Acc Chem Res* 2004, 37:357–364.
37. Roychaudhuri R, Yang M, Hoshi MM, Teplow DB. Amyloid beta-protein assembly and Alzheimer disease. *J Biol Chem* 2009, 284:4749–4753.
38. He X, Giurleo JT, Talaga DS. Role of small oligomers on the amyloidogenic aggregation free-energy landscape. *J Mol Biol* 2009, 395:134–154.
39. McAllister C, Karymov MA, Kawano Y, Lushnikov AY, Mikheikin A, Uversky VN, Lyubchenko YL. Protein interactions and misfolding analyzed by AFM force spectroscopy. *J Mol Biol* 2005, 354: 1028–1042.
40. Carrion-Vazquez M, Oberhauser AF, Fisher TE, Marszalek PE, Li H, Fernandez JM. Mechanical design of proteins studied by single-molecule force spectroscopy and protein engineering. *Prog Biophys Mol Biol* 2000, 74:63–91.
41. Engel A, Muller DJ. Observing single biomolecules at work with the atomic force microscope. *Nat Struct Biol* 2000, 7:715–718.
42. Fisher TE, Marszalek PE, Fernandez JM. Stretching single molecules into novel conformations using the atomic force microscope. *Nat Struct Biol* 2000, 7:719–724.
43. da Silva LP. Atomic force microscopy and proteins. *Protein Pept Lett* 2002, 9:117–126.
44. Hansma HG, Kasuya K, Oroudjev E. Atomic force microscopy imaging and pulling of nucleic acids. *Curr Opin Struct Biol* 2004, 14:380–385.
45. Dufrene YF. Nanoscale exploration of microbial surfaces using the atomic force microscope. *Future Microbiol* 2006, 1:387–396.
46. Hinterdorfer P, Dufrene YF. Detection and localization of single molecular recognition events using atomic force microscopy. *Nat Methods* 2006, 3:347–355.
47. Sewald N, Wilking SD, Eckel R, Albu S, Wollschlager K, Gaus K, Becker A, Bartels FW, Ros R, Anselmetti D. Probing DNA-peptide interaction forces at the single-molecule level. *J Pept Sci* 2006, 12:836–842.
48. Gaboriaud F, Dufrene YF. Atomic force microscopy of microbial cells: application to nanomechanical properties, surface forces and molecular recognition forces. *Colloids Surf B Biointerfaces* 2007, 54:10–19.
49. Giannotti MI, Vancso GJ. Interrogation of single synthetic polymer chains and polysaccharides by AFM-based force spectroscopy. *Chemphyschem* 2007, 8:2290–2307.
50. Herbig ME, Weller KM, Merkle HP. Reviewing biophysical and cell biological methodologies in cell-penetrating peptide (CPP) research. *Crit Rev Ther Drug Carrier Syst* 2007, 24:203–255.
51. Leonenko ZV, Finot E, Cramb DT. Atomic force microscopy to study interacting forces in phospholipid bilayers containing general anesthetics. *Methods Mol Biol* 2007, 400:601–609.
52. Dufrene YF. Towards nanomicrobiology using atomic force microscopy. *Nat Rev Microbiol* 2008, 6:674–680.
53. Engel A, Gaub HE. Structure and mechanics of membrane proteins. *Annu Rev Biochem* 2008, 77:127–148.
54. Helenius J, Heisenberg CP, Gaub HE, Muller DJ. Single-cell force spectroscopy. *J Cell Sci* 2008, 121(Pt 11:):1785–1791.
55. Muller DJ. AFM: a nanotool in membrane biology. *Biochemistry* 2008, 47:7986–7998.
56. Frederix PL, Bosshart PD, Engel A. Atomic force microscopy of biological membranes. *Biophys J* 2009, 96:329–338.
57. Puchner EM, Gaub HE. Force and function: probing proteins with AFM-based force spectroscopy. *Curr Opin Struct Biol* 2009, 19:605–614.
58. Lyubchenko YL, Shlyakhtenko LS, Gall AA. Atomic force microscopy imaging and probing of DNA, proteins, and protein DNA complexes: silatrane surface chemistry. *Methods Mol Biol* 2009, 543:337–351.
59. Evans E. Probing the relation between force—lifetime—and chemistry in single molecular bonds. *Annu Rev Biophys Biomol Struct* 2001, 30:105–128.
60. Bell GI. Models for the specific adhesion of cells to cells. *Science* 1978, 200:618–627.
61. Evans EA, Calderwood DA. Forces and bond dynamics in cell adhesion. *Science* 2007, 316:1148–1153.
62. Evstigneev M, von Gehlen S, Reimann P. Interaction-controlled Brownian motion in a tilted periodic potential. *Phys Rev E Stat Nonlin Soft Matter Phys* 2009, 79(1 Pt 1):011116.
63. Tinoco I Jr, Bustamante C. The effect of force on thermodynamics and kinetics of single molecule reactions. *Biophys Chem* 2002, 101–102:513–533.
64. Krasnoslobodtsev AV, Shlyakhtenko LS, Lyubchenko YL. Probing interactions within the synaptic DNA-SfiI complex by AFM force spectroscopy. *J Mol Biol* 2007, 365:1407–1416.
65. Kransnoslobodtsev AV, Shlyakhtenko LS, Ukraintsev E, Zaikova TO, Keana JF, Lyubchenko YL. Nanomedicine and protein misfolding diseases. *Nanomedicine* 2005, 1:300–305.
66. Stefani M, Dobson CM. Protein aggregation and aggregate toxicity: new insights into protein folding, misfolding diseases and biological evolution. *J Mol Med* 2003, 81:678–699.

67. Spillantini MG, Schmidt ML, Lee VM, Trojanowski JQ, Jakes R, Goedert M. Alpha-synuclein in Lewy bodies. *Nature* 1997, 388:839–840.

68. Spillantini MG, Crowther RA, Jakes R, Hasegawa M, Goedert M. Alpha-Synuclein in filamentous inclusions of Lewy bodies from Parkinson's disease and dementia with lewy bodies. *Proc Natl Acad Sci U S A* 1998, 95:6469–6473.

69. Polymeropoulos MH, Lavedan C, Leroy E, Ide SE, Dehejia A, Dutra A, Pike B, Root H, Rubenstein J, Boyer R, et al. Mutation in the alpha-synuclein gene identified in families with Parkinson's disease. *Science* 1997, 276:2045–2047.

70. Kruger R, Kuhn W, Muller T, Woitalla D, Graeber M, Kosel S, Przuntek H, Epplen JT, Schols L, Riess O. Ala30Pro mutation in the gene encoding alpha-synuclein in Parkinson's disease. *Nat Genet* 1998, 18:106–108.

71. Zarranz JJ, Alegre J, Gomez-Esteban JC, Lezcano E, Ros R, Ampuero I, Vidal L, Hoenicka J, Rodriguez O, Atares B, et al. The new mutation, E46K, of alpha-synuclein causes Parkinson and Lewy body dementia. *Ann Neurol* 2004, 55:164–173.

72. Masliah E, Rockenstein E, Veinbergs I, Mallory M, Hashimoto M, Takeda A, Sagara Y, Sisk A, Mucke L. Dopaminergic loss and inclusion body formation in alpha-synuclein mice: implications for neurodegenerative disorders. *Science* 2000, 287:1265–1269.

73. Feany MB, Bender WW. A Drosophila model of Parkinson's disease. *Nature* 2000, 404:394–398.

74. Uversky VN. Alpha-synuclein misfolding and neurodegenerative diseases. *Curr Protein Pept Sci* 2008, 9:507–540.

75. Tofaris GK, Spillantini MG. Alpha-synuclein dysfunction in Lewy body diseases. *Mov Disord* 2005, 20(suppl 12):S37–S44.

76. Jao CC, Der-Sarkissian A, Chen J, Langen R. Structure of membrane-bound alpha-synuclein studied by site-directed spin labeling. *Proc Natl Acad Sci U S A* 2004, 101:8331–8336.

77. Ulmer JL, Holodny AI. Functional neuroradiology: a call to action. *AJNR Am J Neuroradiol* 2005, 26:2–3.

78. Giasson BI, Murray IV, Trojanowski JQ, Lee VM. A hydrophobic stretch of 12 amino acid residues in the middle of alpha-synuclein is essential for filament assembly. *J Biol Chem* 2001, 276:2380–2386.

79. Heise H, Hoyer W, Becker S, Andronesi OC, Riedel D, Baldus M. Molecular-level secondary structure, polymorphism, and dynamics of full-length alpha-synuclein fibrils studied by solid-state NMR. *Proc Natl Acad Sci U S A* 2005, 102:15871–15876.

80. Uversky VN, Li J, Fink AL. Evidence for a partially folded intermediate in alpha-synuclein fibril formation. *J Biol Chem* 2001, 276:10737–10744.

81. Uversky VN, Kabanov AV, Lyubchenko YL. Nanotools for megaproblems: probing protein misfolding diseases using nanomedicine modus operandi. *J Proteome Res* 2006, 5:2505–2522.

82. Fink AL. The aggregation and fibrillation of alpha-synuclein. *Acc Chem Res* 2006, 39:628–634.

83. Uversky VN, Eliezer D. Biophysics of Parkinson's disease: structure and aggregation of alpha-synuclein. *Curr Protein Pept Sci* 2009, 10:483–499.

84. Tsigelny IF, Bar-On P, Sharikov Y, Crews L, Hashimoto M, Miller MA, Keller SH, Platoshyn O, Yuan JX, Masliah E. Dynamics of alpha-synuclein aggregation and inhibition of pore-like oligomer development by beta-synuclein. *FEBS J* 2007, 274:1862–1877.

85. Tsigelny IF, Sharikov Y, Miller MA, Masliah E. Mechanism of alpha-synuclein oligomerization and membrane interaction: theoretical approach to unstructured proteins studies. *Nanomedicine* 2008, 4:350–357.

86. Lee JH, Lee IH, Choe YJ, Kang S, Kim HY, Gai WP, Hahn JS, Paik SR. Real-time analysis of amyloid fibril formation of alpha-synuclein using a fibrillation-state-specific fluorescent probe of JC-1. *Biochem J* 2009, 418:311–323.

87. Ban T, Hamada D, Hasegawa K, Naiki H, Goto Y. Direct observation of amyloid fibril growth monitored by thioflavin T fluorescence. *J Biol Chem* 2003, 278:16462–16465.

88. Kaylor J, Bodner N, Edridge S, Yamin G, Hong DP, Fink AL. Characterization of oligomeric intermediates in alpha-synuclein fibrillation: FRET studies of Y125W/Y133F/Y136F alpha-synuclein. *J Mol Biol* 2005, 353:357–372.

89. Yu J, Malkova S, Lyubchenko YL. Alpha-synuclein misfolding: single molecule AFM force spectroscopy study. *J Mol Biol* 2008, 384:992–1001.

90. Yu J, Lyubchenko YL. Early stages for Parkinson's development: alpha-synuclein misfolding and aggregation. *J Neuroimmune Pharmacol* 2009, 4:10–16.

91. Dietz H, Rief M. Exploring the energy landscape of GFP by single-molecule mechanical experiments. *Proc Natl Acad Sci U S A* 2004, 101:16192–16197.

92. Dietz H, Rief M. Protein structure by mechanical triangulation. *Proc Natl Acad Sci U S A* 2006, 103:1244–1247.

93. Collinge J, Clarke AR. A general model of prion strains and their pathogenicity. *Science* 2007, 318:930–936.

94. Silveira JR, Raymond GJ, Hughson AG, Race RE, Sim VL, Hayes SF, Caughey B. The most infectious prion protein particles. *Nature* 2005, 437:257–261.

95. Rubinstein A, Lyubchenko YL, Sherman S. Dynamic properties of pH-dependent structural organization of

the amyloidogenic beta-protein (1–40). *Prion* 2009, 3:31–43.

96. Marcon G, Plakoutsi G, Canale C, Relini A, Taddei N, Dobson CM, Ramponi G, Chiti F. Amyloid formation from HypF-N under conditions in which the protein is initially in its native state. *J Mol Biol* 2005, 347:323–335.
97. Brucale M, Sandal M, Di Maio S, Rampioni A, Tessari I, Tosatto L, Bisaglia M, Bubacco L, Samori B. Pathogenic mutations shift the equilibria of alpha-synuclein single molecules towards structured conformers. *Chembiochem* 2009, 10:176–183.
98. Sandal M, Valle F, Tessari I, Mammi S, Bergantino E, Musiani F, Brucale M, Bubacco L, Samori B. Conformational equilibria in monomeric alpha-synuclein at the single-molecule level. *PLoS Biol* 2008, 6:e6.
99. Balbirnie M, Grothe R, Eisenberg DS. An amyloid-forming peptide from the yeast prion Sup35 reveals a dehydrated beta-sheet structure for amyloid. *Proc Natl Acad Sci U S A* 2001, 98:2375–2380.
100. Merkel R, Nassoy P, Leung A, Ritchie K, Evans E. Energy landscapes of receptor-ligand bonds explored with dynamic force spectroscopy. *Nature* 1999, 397:50–53.
101. Shankar GM, Li S, Mehta TH, Garcia-Munoz A, Shepardson NE, Smith I, Brett FM, Farrell MA, Rowan MJ, Lemere CA, et al. Amyloid-beta protein dimers isolated directly from Alzheimer's brains impair synaptic plasticity and memory. *Nat Med* 2008, 14:837–842.
102. Hu NW, Smith IM, Walsh DM, Rowan MJ. Soluble amyloid-beta peptides potently disrupt hippocampal synaptic plasticity in the absence of cerebrovascular dysfunction in vivo. *Brain* 2008, 131(Pt 9):2414–2424.
103. Cerf E, Sarroukh R, Tamamizu-Kato S, Breydo L, Derclaye S, Dufrene YF, Narayanaswami V, Goormaghtigh E, Ruysschaert JM, Raussens V. Antiparallel beta-sheet: a signature structure of the oligomeric amyloid beta-peptide. *Biochem J* 2009, 421:415–423.
104. Tycko R, Sciarretta KL, Orgel JP, Meredith SC. Evidence for novel beta-sheet structures in Iowa mutant beta-amyloid fibrils. *Biochemistry* 2009, 48:6072–6084.
105. Rangachari V, Moore BD, Reed DK, Sonoda LK, Bridges AW, Conboy E, Hartigan D, Rosenberry TL. Amyloid-beta(1–42) rapidly forms protofibrils and oligomers by distinct pathways in low concentrations of sodium dodecylsulfate. *Biochemistry* 2007, 46:12451–12462.
106. Sgourakis NG, Yan Y, McCallum SA, Wang C, Garcia AE. The Alzheimer's peptides Abeta40 and 42 adopt distinct conformations in water: a combined MD/NMR study. *J Mol Biol* 2007, 368:1448–1457.
107. Kim J, Lee M. Observation of multi-step conformation switching in beta-amyloid peptide aggregation by fluorescence resonance energy transfer. *Biochem Biophys Res Commun* 2004, 316:393–397.
108. Petkova AT, Yau WM, Tycko R. Experimental constraints on quaternary structure in Alzheimer's beta-amyloid fibrils. *Biochemistry* 2006, 45:498–512.
109. Chimon S, Shaibat MA, Jones CR, Calero DC, Aizezi B, Ishii Y. Evidence of fibril-like beta-sheet structures in a neurotoxic amyloid intermediate of Alzheimer's beta-amyloid. *Nat Struct Mol Biol* 2007, 14:1157–1164.
110. Lakowicz JR: *Principles of Fluorescence Spectroscopy*. Singapore: Springer; 2006.
111. Andrews JM, Roberts CJ. A Lumry-Eyring nucleated polymerization model of protein aggregation kinetics: 1. Aggregation with pre-equilibrated unfolding. *J Phys Chem B* 2007, 111:7897–7913.
112. Orte A, Birkett NR, Clarke RW, Devlin GL, Dobson CM, Klenerman D. Direct characterization of amyloidogenic oligomers by single-molecule fluorescence. *Proc Natl Acad Sci U S A* 2008, 105:14424–14429.
113. Serio TR, Cashikar AG, Kowal AS, Sawicki GJ, Moslehi JJ, Serpell L, Arnsdorf MF, Lindquist SL. Nucleated conformational conversion and the replication of conformational information by a prion determinant. *Science* 2000, 289:1317–1321.
114. Lai Z, Colon W, Kelly JW. The acid-mediated denaturation pathway of transthyretin yields a conformational intermediate that can self-assemble into amyloid. *Biochemistry* 1996, 35:6470–6482.
115. Ding TT, Lee SJ, Rochet JC, Lansbury PT Jr. Annular alpha-synuclein protofibrils are produced when spherical protofibrils are incubated in solution or bound to brain-derived membranes. *Biochemistry* 2002, 41:10209–10217.
116. Lin H, Bhatia R, Lal R. Amyloid beta protein forms ion channels: implications for Alzheimer's disease pathophysiology. *FASEB J* 2001, 15:2433–2444.
117. Jang H, Arce FT, Capone R, Ramachandran S, Lal R, Nussinov R. Misfolded amyloid ion channels present mobile beta-sheet subunits in contrast to conventional ion channels. *Biophys J* 2009, 97:3029–3037.
118. Jang H, Ma B, Lal R, Nussinov R. Models of toxic beta-sheet channels of protegrin-1 suggest a common subunit organization motif shared with toxic alzheimer beta-amyloid ion channels. *Biophys J* 2008, 95:4631–4642.
119. Lal R, Lin H, Quist AP. Amyloid beta ion channel: 3D structure and relevance to amyloid channel paradigm. *Biochim Biophys Acta* 2007, 1768:1966–1975.
120. Jang H, Arce FT, Ramachandran S, Capone R, Azimova R, Kagan BL, Nussinova R, Lal R. Truncated beta-amyloid peptide channels provide an alternative mechanism for Alzheimer's disease and Down syndrome. *Proc Natl Acad Sci U S A* 2010, 107:6538–6543.

